Change of optical responses of Au nanoparticles induced by high-energy Si ion-irradiations

Sachin K. Srivastava*, Parthasarathi Gangopadhyay, S. Amirthapandian,P. Magudapathy, Shyamala R. Polaki, Binay K. Panigrahi, T. N. Sairam

Materials Science Group, Indira Gandhi Centre for Atomic Research, Kalpakkam 603102, India

*Corresponding author; Tel.: (+91) 4427480500; E-mail: sachin@igcar.gov.in

Received: 31 March 2016, Revised: 30 September 2016 and Accepted: 20 April 2017

DOI: 10.5185/amp.2017/040
www.vbripress.com/amp

Abstract

Au nanoparticles onto a silica-glass (SiO_2) surface have been formed due to thermal dewetting of Au thin films. Subsequently, high energy Si ion-irradiations on the pristine Au nanoparticles result systematic redshifts of optical responses and concomitant broadening of the optical absorption peaks with the increase of ion doses. Essentially, these phenomena have been explained in the light of ion-beam mixing and transient molten-state diffusion process of Au atoms in the underneath SiO_2 substrate. Analysis of high resolution electron microscopy and Rutherford backscattering data have corroborated the ion-beam induced mixing of Au atoms with the silica glass.

Keywords: Au nanoparticles, ion-irradiation, optical response, electron microscopy, RBS.

Introduction

In recent times, various types of plasmonic substrates (particularly nanoscaled metal particles on dielectric substrates) have been developed for many applications like SERS [**1**], optical tweezers [**2**], photoluminescence enhancement [**3**], sub diffraction limit imaging [**4**], solar cell performance enhancement by light trapping [**5**] and fast optical switching [**6**]. These applications crucially depend on shape, size and distribution of metal nanoparticles on the substrates [**7**]. The plasmonic substrates have been prepared, as reported earlier, through lithographic processes, masked deposition and by chemical synthesis [**8**]. Controlled fine tuning of plasmonic response of such substrates is expected to enhance these application properties regarding optical switching, Photoluminescence and SERS. This has been achieved by varying shape, sizes and arrangement of metal nanostructures on a substrate [**8**]. Especially, the interfaces of the substrate with the metal nanostructures play an important role in the optical response of the plasmonic substrates [**9**]. The interface of the nanostructure with the substrate can be tailored by ion irradiation for fine tuning of the plasmonic response.

Ion irradiation is a versatile technique to synthesize and modify nanoparticles on matrices, and can easily be adapted as a technology of choice for the creation of smart materials. Use of ion irradiation has further distinct advantages: species are usually buried in the subsurface and hence chemically clean, superior control over composition, size and shape distributions, and not limited by the solubility factor of the matrix [**10**]. Also, bombarded ions of high energy get embedded into the matrix at depths far away from the surface and hence the composition of surface coatings remains unchanged [**11**]. Ion beams have been used to modify sizes and shapes of metal nanostructures which results in modification of plasmonic response of metal nanoparticles [**12**]. Here, in this article, we report controlled tuning of optical responses of Au nanoparticles on the surface of silica glass by high energy Si^{5+} ion irradiation. In addition to ion-beam techniques, there are various methods to modify shapes and sizes of different metal nanoparticles (**Table 1** enlists some of it).

Detailed study about the ion beam irradiation of Au nanoparticles and related changes in the interface of the substrate with Au nanoparticles has been reported in the present paper. Various experimental (optical absorption spectroscopy, Rutherford backscattering spectrometry, electron microscopy) results have been analyzed to elucidate the changes in optical response of Au nanoparticles upon ion irradiation. Underlying mechanism of ion-beam interaction with Au nanoparticles and mixing at the interface of nanoparticles-silica substrate has been discussed.

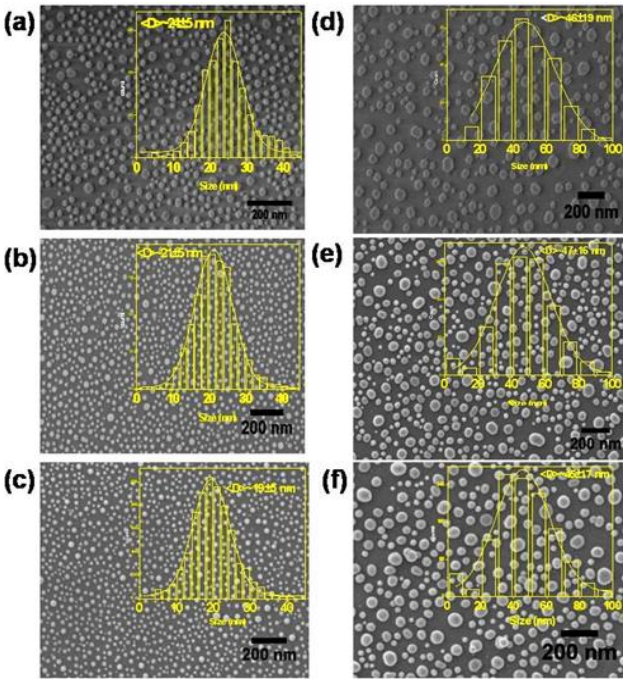

Fig. 1.SEM images are shown for thermally annealed and ion irradiated Au/SiO_2 samples. Left column is for 2.5 nm thick Au films on a silica glass, where samples are: (a) annealed for 1 hr at 800 $^{\circ}$C in Ar gas, subsequently 8 MeV Si^{5+} irradiated with ion doses (b) 3×10^{15} ions/cm^2 and (c) 6×10^{15} ions/cm^2. Right column shows 5 nm thick Au films on a silica glass, where samples are: (d) annealed for 1 hr at 800 $^{\circ}$C in Ar gas, subsequently 8 MeV Si^{5+} ion irradiated with doses (e) 3×10^{15} ions/cm^2 and (f) 6×10^{15} ions/cm^2. Overlaid graphs show the corresponding size histograms of Au nanoparticles, and Gaussian fits estimate average size of Au nanoparticles in various samples.

Experimental

Gold (Au) films of thicknesses 2.5 and 5.0 nm were deposited on cleaned silica-glass substrates by thermal evaporation method. Thickness of Au films, during the deposition, was measured using a quartz crystal monitor. The evaporation chamber was evacuated to a base pressure of ~10^{-6} mbar. Subsequently, Au films were thermally annealed for 1 hr at 800 $^{\circ}$C in Ar gas atmosphere for the dewetting to take place. These annealed samples were subsequently irradiated with 8 MeV Si^{5+} ions with doses up to 6×10^{15} ions/cm^2. Scanned ion-beam over an area ~1 cm^2 was used for a uniform irradiation on these samples in a high vacuum chamber (~10^{-7} mbar). Depth-profiling of Au atoms in thermally annealed and ion irradiated samples has been measured by Rutherford backscattering spectrometry (RBS). Surface barrier solid state detector kept at scattering angle of 165^{o} was used for the detection of the backscattered He^{+} ions. Ion-beam irradiations and RBS measurements were carried out with the 1.7 MV Tandetron accelerator. A dual-beam spectrophotometer (Shimadzu PC 3101) was used to record optical absorption spectra of these samples. Plain silica-glass substrate was kept on the reference beam line during the collection of optical absorption spectra. Surface morphological changes due to thermal annealing and subsequent ion-beam irradiations were analyzed by field-emission scanning electron microscope (FESEM, Zeiss SUPRA 55). SEM images have been analyzed using the ImageJ software [**13**]. In addition, transmission electron microscope (Libra 200 FE Zeiss) was used to examine the ion-beam mixed region of the silica substrate. Post-irradiated Au/SiO_2 samples were kept for 1 min in an aqua-regia solution to remove remnant unmixed Au metal on the silica substrate.

Table 1. Selected methods for synthesis, and controlling sizes & shapes of metal nanoparticles.

Methods of synthesis	Materials	Article references
Inert Gas Condensation	Metal-graphene core shell nanoparticles	Sengar, S. K.; Mehta, B. R.; Kumar, R.; Singh, V.; *Sci. Rep.*, **2013,** 3, 2814. DOI:10.1038/srep02814
Swift heavy ion irradiation	Au nanoparticles	Mishra, Y. K.; Singh, F.; Avasthi, D. K.; Pivin, J. C.; Pippel, E.; *Appl. Phys. Lett.*, **2007**, 91, 063103. DOI: 10.1063/1.2764556
Chemical processes	Metal Nanoparticles	An, K.; Somorjai, G. A.; *ChemCatChem*, **2012**, 4, 1512. **DOI**: 10.1002/cctc.201200229
Pulsed Laser irradiation	Au nanoparticles	Grochowska, K.; Śliwiński, G.; Iwulska, A.; Sawczak, N.; Nedyalkov, P.; Atanasov, G.; Obara, M.; *Plasmonics*, **2013,** 8, 105. **DOI**:10.1007/s11468-012-9428-3
Magnetron sputtering	Ni Nanoparticles	Peng, T.; Xiao, X.; Wu, W.; Jiang, C. Z.; *J. Mater. Sci.*, **2012**, 47, 508. **DOI:** 10.1007/s10853-011-5827
High-temperature reductive decompositio n	Ni Nanoparticles	He, X.; Zhong, W.; Chak-Tong, A.; Du, Y.; *Nanoscale Res. Lett.*, **2013,** 8, 446. **DOI**: 10.1186/1556-276X-8-446
Mechanical attrition (e.g., ball milling)	Fe nanoparticles	Muñoz, J.; Cervantes, J.; Esparza, R.; Rosas, G.; *Nanopart. Res.*, **2007**, 9, 945. **DOI**: 10.1007/s11051-007-9226-6

Results and discussion

Pristine Au metal nanoparticles (approximately of uniform sizes on silica substrate) have been observed after thermal annealing Au/SiO_2 samples. Formation of Au nanoparticles is understood as a result of thermal

dewetting of Au thin films on a silica substrate due to the annealing [**14**, **15**]. **Fig. 1**(a) and **1(d)** displays SEM images as well as corresponding size histograms of Au nanoparticles on silica formed upon annealing Au thin films of thickness 2.5 and 5.0 nm, respectively. Average sizes of Au nanoparticles have been obtained from the Gaussian fitting (shown as overlay in **Fig. 1**) of size-histograms. Sizes of Au nanoparticles are found to be 24±5 and 46±18 nm respectively for thermally annealed 2.5 and 5.0 nm Au films. Small reduction in sizes of Au nanoparticles have been observed for 2.5 nm thick Au film sample after the Si^{5+} ion irradiations (with doses 3×10^{15} and 6×10^{15} ions/cm^2, shown in **Fig. 1**(b, c), respectively). Compared to 2.5 nm Au films, average sizes of Au nanoparticles remain almost unchanged after the Si^{5+} ion irradiations of thermally annealed 5.0 nm Au films on silica (see **Fig. 1**(d) to **1**(f)). The fact implies that relative loss of Au atoms (due to ion-beam induced mixing and sputtering) from larger nanoparticles (average size ~ 46 nm) was negligibly small compared to relative loss of Au atoms from smaller Au nanoparticles (average size ~ 24 nm) on the silica substrate. Areal coverage of Au on silica surface for the annealed films are around 25 and 35% for 2.5 and 5 nm films, respectively. In fact, no significant change of areal coverage of Au has been measured after Si ion irradiations. Cross-sectional SEM measurements have been carried out to examine the morphological changes of Au nanoparticles on the glass substrate as a result of Si^{5+} ion irradiations. Cross-sectional images (see **Fig. 2**) reveal that the height to base ratio of Au nanoparticles remained close to 0.5, before and after the Si^{5+} ion irradiations. The result implies that shape of supported Au nanoparticles after the Si^{5+} ion irradiations remained unchanged.

Optical absorption spectra of pristine and Si^{5+} ion irradiated Au nanoparticles are displayed in **Fig. 3**(a) and **3**(b). Characteristic surface-plasmon resonance (SPR) absorption peak around 525 nm (**Fig. 3**(a) and **3**(b), solid line) confirms the formation of Au nanoparticles on the silica-glass surface after the annealing of Au films. In both the cases, a systematic red shift of the optical absorption peak along with concomitant peak-broadening with increase of Si^{5+} ion doses has been observed (**Fig. 3**(a) and 3(b), symbols). Positions of the resonances and full-width at half-maximum (FWHM) values for thermally annealed and subsequently ion irradiated samples are provided in **Table 2**. It may be noticed here that the quantum of shift and FWHM of the peak absorption for same ion dose has increased with increase of Au film thickness. Position of the optical absorption peak of nanoparticles crucially depends on dielectric constant of the host medium, sizes and shapes of the nanoparticles [**9**]. For spherical Au nanoparticles on a silica glass, SPR absorption peak has been observed around 530 nm [**12**]. Usually, peak position for optical absorption shows red shift with increase of sizes and change in shape of Au nanoparticles [**9**, **16**]. However, SEM images (**Fig. 1**) show that sizes of Au nanoparticles are either reducing (for 2.5 nm Au films) or remain same (for 5 nm Au films) upon Si^{5+} ion irradiations. Also, cross-sectional SEM images (**Fig. 2**) show no significant change of shape of Au nanoparticles upon Si^{5+} ion irradiations. Thus, as we understand, the observed red shift may not be due to change in size or shape of the supported Au nanoparticles on the surface of silica substrates.

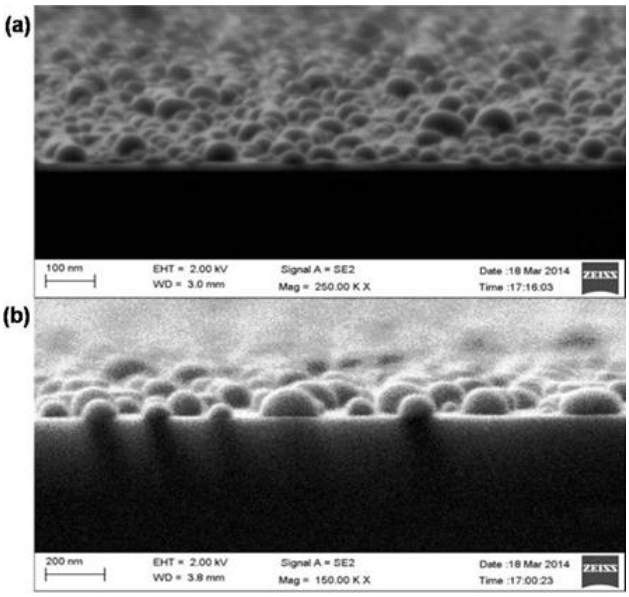

Fig. 2. Cross-sectional SEM images of thermally annealed 5 nm Au film on a silica glass are shown here for (a) as annealed, (b) subsequently irradiated by 8 MeV Si^{5+} ions with doses 6×10^{15} ions/cm^2. Images reveal that shape of Au nanoparticles remained unchanged after the ion irradiation. The height to base ratio of Au nanoparticles remains around 0.5 before and after the ion irradiation.

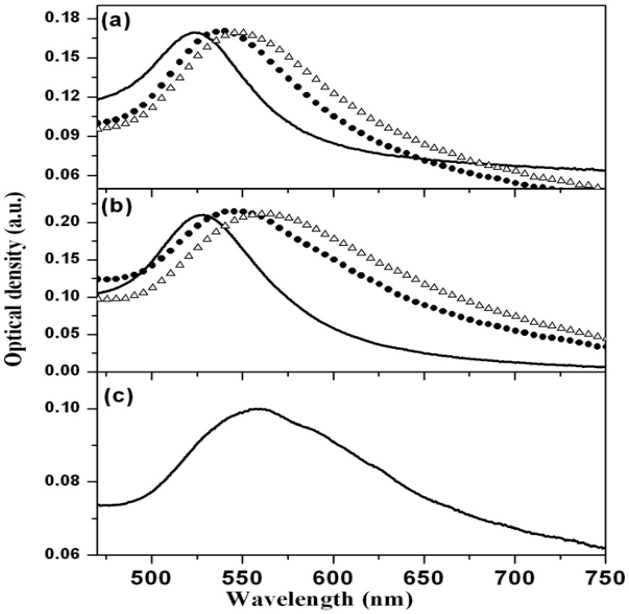

Fig. 3. Optical absorption spectra of Au nanoparticles after thermal annealing (solid line) for (a) 2.5 nm and (b) 5 nm thick Au films on silica, and upon subsequent 8 MeV Si^{5+} ion irradiations with different doses (●: 3×10^{15}, Δ: 6×10^{15} ions/cm^2). A systematic red shift with increase of ion doses may be noticed. (c) Thermally annealed 5 nm thick Au films on silica, subsequently 8 MeV Si^{5+} ion irradiated with dose 3×10^{15} ions/cm^2 ions, and after etching with aqua-regia.

As we know, under the quasi-static size approximation ($2R<\lambda_{max}/10$) (λ_{max}being the position for dipolar resonance absorption), the frequency of collective oscillation (ω_{res}) of free electrons in metal nanoparticles may be written as [**9**],

$$\omega_{res}^2 = \frac{\omega_p^2}{1+2\varepsilon_m} \quad (1)$$

ω_p is the plasma frequency in bulk metal and ε_m is the dielectric constant of the host medium; ω_{res} depends strongly on ω_p and ε_m (see Eq.1). The optical absorption peak (λ_{res}) due to the SPR in metal nanoparticles thus may shift towards higher wavelengths with an increase of dielectric constant of the host medium. Compared to the pristine samples, observed red shift of the SPR (**Fig. 3**(a) and **3**(b)) of Au nanoparticles upon Si ion irradiation is very interesting.

In the present case, ion-beam induced mixing of supported Au nanoparticles with the silica matrix plays a very important role and will be discussed in the subsequent section along with the RBS results. Compared to the pristine supported Au nanoparticles (with incomplete embedding), Au nanoparticles in the ion-irradiated samples may experience an increase of effective dielectric constant. Increase of effective dielectric constant around the metal atoms is likely as Au nanoparticles are completely embedded in post ion-irradiated samples. Ion-beam induced mixing is thought to be as the basic mechanism in the present case leading to the formation of embedded Au nanoparticles in a silica matrix. This has been further elucidated by the RBS and HRTEM measurements. Hence, the observed red shift of SPR peak is due to formation of embedded Au nanoparticles upon irradiation. Ion-beam mixed amount of Au atoms directly varies to the square root of the ion doses [**17**]. Hence, the volume fraction of embedded Au nanoparticles into a silica matrix may increase with increase of Si ion doses. With more amounts of Au atoms into the silica matrix with increasing ion doses, the average size/number density of Au nanoparticles is likely to increase. It is well known that SPR of Au nanoparticles shifts towards higher wavelength with increase in particle size and number density [**9**, **18**]. This may be the reason behind the red shift of SPR peak upon further irradiation (3×10^{15} ions/cm^2 to 6×10^{15} ions/cm^2). This explains the systematic red shift of SPR absorption peak with increase of ion doses (see **Fig. 3**(a) and **3**(b)).

Fig. 3(c) shows the optical absorption of thermally annealed 5 nm Au film after the etching. Interestingly, SPR of Au nanoparticles has not been suppressed completely as in the case of only thermally annealed sample. This shows the presence of Au nanoparticles embedded into the silica matrix after high energy Si^{5+} ion irradiations. This is further supported by RBS and TEM measurements. SPR of embedded nanoparticles occur at higher wavelength compared to supported nanoparticles due to increase in dielectric constant of host medium [**9**, **18**]. Hence, the SPR absorption peak wavelength in present case is expected to appear at higher wavelength because of contribution from embedded Au nanoparticles. SPR peak of Au nanoparticles has not been observed after the etching (not shown here). This confirms that Au surface layers have been completely removed from the silica surface by the etching process.

Frequent collisions and scattering of free electrons over the surface of metal nanoparticles plays a decisive role in controlling the width of the surface-plasmon resonance. Collisions and scattering is likely to be enhanced in small metal particles as the mean free path of the electrons is much restricted due to the reduced physical dimension of the metal nanoparticles [**19, 20**]. The mean free path of free electrons in Ag and Au metal, for example, is about 40-50 nm [**21**]. Due to physical restrictions of metal nanoparticles, coherence of collective oscillations may be hindered and increase of collisional broadening is likely. As a consequence, band width of the surface-plasmon resonance increases with decreasing radius of metal nanoparticles. Following classical Drude model in metal nanoparticles, this fact may be described mathematically as,

$$\gamma = \gamma_{bulk} + \frac{Av_F}{R} \quad (2)$$

R is the particle radius, γ being the damping and v_F is the Fermi velocity of electrons in metals (~ 1.4×10^6 ms^{-1} in Au [**22**]); γ_{bulk}represents the damping in bulk metals. The constant A is a fitting coefficient whose value depends on the surrounding host material. The value of Av_F is ~ 0.35 and 0.90 eV-nm for Ag or Au nanoparticles in air and in silica, respectively [**9**]. In the present case, where pristine Au nanoparticles were irradiated with high energy Si ions, increase of γ may be expected, according to Eq. 2, due to formation of fine ($\gamma\sim\frac{1}{R}$) and embedded (increase of Av_F) Au nanoparticles.

Table 2. SPR peak positions of Au nanoparticles and associated FWHM values of thermally annealed and Si^{5+} ion-irradiated assemblies of the nanoparticles are enlisted.

Thickness of Au Films (nm)	Post-irradiation doses on annealed samples (ions/cm^2)	SPR peak position/FWHM (nm)
2.5	Annealed	525/58
	3×10^{15}	541/82
	6×10^{15}	551/95
5.0	Annealed	527/60
	3×10^{15}	550/103
	6×10^{15}	565/132

As discussed later, average size of embedded Au nanoparticles in silica is indeed found to be very small (2 nm, see **Fig. 4**). Hence, the observed increase of band width of SPR resonance with increase of ion doses (see **Fig. 3**(a) and **3**(b)) is ascribed due to an enhanced

damping with the formation of small embedded Au nanoparticles in a silica matrix. Further, to examine optical response of embedded Au nanoparticles, one of the samples was etched with aqua-regia for removal of the metal on the silica glass substrate. Recorded optical absorption spectra of Au nanoparticles in a silica glass are shown in **Fig. 3**(c). Band width of the SPR resonance is fairly large (see **Table 2**) for the embedded Au nanoparticles. The result further confirms fine size of Au nanoparticles. As influx of Au atoms in silica increases with increase of Si ion doses (e.g., 6×10^{15} ions/cm^2), inter-particle distances of fine sized Au nanoparticles is expected to decrease. Observed additional broadening of the surface-plasmon resonance absorption in the present case is further attributed to an increase of the local field fluctuations due to multiple interactions among the high-density Au nanoparticles that are embedded randomly in the glass matrix. As a result of these interactions, Au nanoparticles present in the glass may support the surface-plasmon resonance absorptions over a broad range of incident photon energies. The trends observed in the numerical study support the present optical absorption experimental results as well [**23**].

Transmission electron microscopy (TEM) measurements have been carried out on this particular sample (details of the sample: 5 nm thick Au film was thermally annealed and subsequently Si^{5+} ion irradiated with dose 3×10^{15} ions/cm^2 and then etched by the aqua-regia solution) to examine the state of diffused Au atoms in the silica matrix. TEM results reveal that diffused Au atoms form nanoparticles in the silica matrix (see **Fig. 4** (a)). This corroborates with optical absorption spectroscopy results. The Gaussian distribution fit of size-histogram shows Au nanoparticles with average size 2 nm (**Fig. 4**(b)). The selected area electron diffraction pattern reveals the crystal structure of Au nanoparticles as face centered cubic (*fcc*) type. Diffraction spots are indexed with the corresponding (*hkl*) planes (inset, **Fig. 4** (a)).

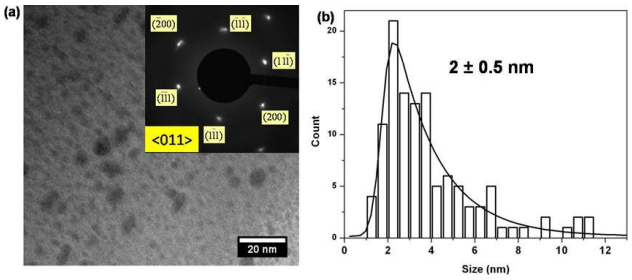

Fig. 4. (a) TEM image shows embedded Au nanoparticles in this sample (thermally annealed (800 °C, 1 hr) Au (5 nm)/ SiO_2 film was irradiated with dose 3×10^{15} ions/cm^2 of 8 MeV Si^{5+} ions and etched by aqua-regia acid solution). The image shows isolated Au nanoparticles. The inset shows electron diffraction pattern indexed with the corresponding plane. The crystal structure is found to be face centered cubic (*fcc*) type with zone axis as <011>. Size histogram fitted with Gaussian distribution of Au nanoparticles is shown in (b).

Primarily, RBS studies have been performed to highlight the ion beam mixing of Au nanoparticles with the silica matrix. RBS measurements of 5 nm Au film after thermal annealing and subsequent Si^{5+} ion irradiations have been carried out and RBS spectra is shown in the inset of **Fig. 5**. No significant change in Au peak area before and after the Si^{5+} ion irradiations implies that loss of Au atoms from samples due to ion beam sputtering is negligibly small. However, because of the roughness of Au film samples and with a moderate detector resolution (~15 keV), it is difficult to comment on mixing of gold in silica. Hence, to study ion beam mixing of Au into silica, the surface Au has been removed while keeping the sample in the aqua-regia solution for one minute. A pristine silica surface (devoid of Au atoms) after the etching is expected [**24**]. RBS spectrum (drawn in blue) of this sample (etched 5 nm thick Au film) is shown in **Fig. 5** confirming the complete removal of Au metal. RBS measurement has been also carried out on a different sample (details of the sample: 5 nm thick Au film was thermally annealed and subsequently Si^{5+} ion irradiated with dose 3×10^{15} ions/cm^2 and then etched by the aqua-regia solution) to study the ion-beam mixing. In this sample, RBS yield from Au atoms is observed (see **Fig. 5**, drawn in red) revealing presence of Au atoms inside the silica matrix. Also, backscattering counts near the Si surface edge in the spectrum (shown in red, **Fig. 5**) is less compared to etched Au film on silica (shown in blue, **Fig. 5**). This shows mixing of Au into the silica matrix during the Si^{5+} ion irradiations. RBS data have been fitted with SIMNRA software [**25**]. Presence of Au atoms has been estimated up to a depth of 150 nm into the silica matrix. Areal density of Au atoms into the silica matrix is worked out to be ~7×10^{16} atoms/cm^2. The calculated rate of mixing ($\frac{\Delta\sigma^2}{\emptyset}$) is ~ 375 nm^4 for the Si^{5+} ion dose 6×10^{15} ions/cm^2. In the present case, calculated high rate of mixing occurs as a result of transient molten-state diffusion during thermal spike and this phenomenon has been discussed in earlier reports [**11, 17**].

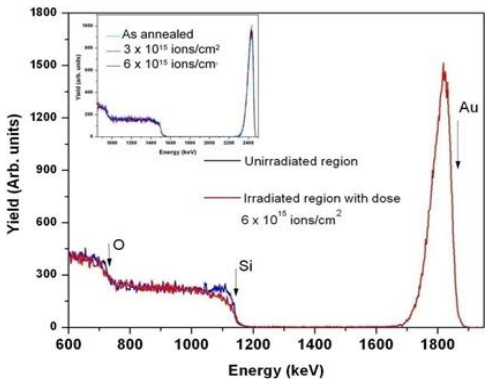

Fig. 5. RBS spectra of 5 nm thick Au films on silica after thermal annealing and subsequently etched by aqua-regia solution (blue line). RBS spectra of 5 nm thick Au films on silica upon thermal annealing and subsequently irradiated by 8 MeV Si^{5+} ions with dose 6×10^{15} ions/cm^2 and finally etched by aqua-regia solution (red line). A fraction of RBS yield at the Si edge (1000- 1200 keV) is missing in the irradiated sample, indicating the mixing of Au with silica during the ion irradiations. Arrows represent the surface edge of respective elements. He^+ ions of energy 2 MeV were used for the RBS measurements. Inset figure shows the RBS spectra (He^+ ions of energy 2.5 MeV used) of 5 nm thick Au films on the silica-glass upon thermal annealing and subsequent irradiation by 8 MeV Si^{5+} ions with different ion doses.

Conclusion

Au nanoparticles have been synthesized on a silica-glass surface by thermal annealing of Au thin films. High energy Si^{5+} ion irradiations on the supported Au nanoparticles resulted in the ion-beam mixing of Au into the silica matrix. The electric field intensity gets enhanced due to reduced dimensions of metal structures on dielectric materials; the technique may be applied for synthesizing platform to study surface enhanced Raman spectroscopy of materials. Also, photothermal effect of Au nanoparticles on silica may provide a source of heat in thermoelectric applications, like in the solar technologies for improved light absorption.

Author's contributions

Conceived the plan: S. K. Srivastava; Performed the expeirments: S. K. Srivastava, S. Amirthapandian, P. Magudapathy, S. R. Polaki, T. N. Sairam; Data analysis: S. K. Srivastava, P. Gangopadhyay,B. K. Panigrahi; Wrote the paper: S. K. Srivastava, P. Gangopadhyay. Authors have no competing financial interests.

References

1. Jeon, T. Y.; Kim, D. J.; Park, S.; Kim, S.; and Kim, D.; *Nano Convergence*, **2016,** 3, 18. **DOI**:10.1186/s40580-016-0078-6
2. Petrov, M. I.; Sukhov, S. V.; Bogdanov, A. A.; Shalin, A. S; Dogariu, A.; *Laser Photonics Rev.*, **2016**, 10, 116. **DOI**:10.1002/lpor.201500173
3. Lumdee, C.; Yun, B., Kik, P. G.; *ACS Photonics*, **2014**, 1, 1224. **DOI**: 10.1021/ph500304v
4. Olson, A. P.; Ertsgaard, C. T.; Elliott, S. N.; Lindquist, N. C.; *ACS Photonics*, **2016**, 3, 329. **DOI**: 10.1021/acsphotonics.5b00647
5. Ouyang, Z.; Zhao, X.; Varlamov, S.; Tao, Y.; Wong, J.; Pillai, S.; *Prog. Photovolt: Res. Appl*., **2011**, 19, 917. **DOI**: 10.1002/pip.1135
6. Muskens, O. L.; Bergamini, L.; Wang, Y.; Gaskell, J. M.; Zabala, N.; de Groot, C.; Sheel, D. W.; Aizpurua, J.; *Light: Sci. Appl.*, **2016,** 5, e16173 **DOI**: 10.1038/lsa.2016.173
7. Sharma, B.; Cardinal, M. F.; Kleinman, S. L.; Greeneltch, N. G.; Frontiera, R. R.; Blaber, M. G.; Schatz, G. C.; Duyne R. P. V.; *MRS Bull.*, **2013,** 38, 615. **DOI**: 10.1557/mrs.2013.161
8. Wang, A. X.; Kong, Xianming K.; *Materials*,**2015**, 8, 3024. **DOI**: 10.3390/ma8063024
9. Kreibig, U.; and Vollmer, M.;Optical Properties of Metal Clusters, Springer, Berlin, **1995.** **DOI**: 10.1007/978-3-662-09109-8
10. Jain, I. P.; Agarawal, G.; *Surf. Sci. Rep.*, **2011**, 66, 77. **DOI**: 10.1016/j.surfrep.2010.11.001
11. Srivastava, S.K.; Avasthi, D. K.; Assaman, W.; Wang, Z. G.; Kucal, H.; Jacquet, E.; Carstanjen, H.D.; and Toulemonde, M.; *Phys. Rev. B*, **2005**, 71, 193405. **DOI**: 10.1103/PhysRevB.71.193405
12. Gangopadhyay, P. ; Srivastava, S. K. ; Magudapathy, P. ; Sairam, T.N. ; Nair, K.G.M. ; and Panigrahi, B.K.; *Vacuum*, **2010**, 84, 1411. **DOI**: 10.1016/j.vacuum.2010.01.013
13. Schneider, C.A.; Rasband, W.S.; and Eliceiri, K.W.; *Nat. Methods*, **2012,** 9, 676. **DOI**: 10.1038/nmeth.2019
14. Mullins, W. W.; *J Appl. Phys.*, **1957**, 28, 333. **DOI**: 10.1063/1.1722742
15. Shaffir, E.; Riess, I.; and Kaplan, W. D.; *Acta Mater*., **2009,** 57, 248. **DOI**: 10.1016/j.actamat.2008.09.004
16. Huang, X.; El-Sayed, M. A.; *J. Adv. Res.*, 2010, 1, 13. **DOI** : 10.1016/j.jare.2010.02.002
17. Bolse, W.; Schattat, B. ; *Nucl. Instrum. Methods Phys. Res., Sect. B*, **2003**, 209, 32. **DOI**: 10.1016/S0168-583X(02)02039-6
18. Noguez, C. ; *J. Phys. Chem. C*, **2007**, 111, 3806. **DOI**:10.1021/jp066539m
19. Kreibig, U.; and Fragstein, C. V.; *Z. Phys*., **1969**, 224, 307. **DOI**: 10.1007/BF01393059
20. Kreibig, U.; *Z. Phys.*, **1970**, 234, 307. **DOI**: 10.1007/BF01394718
21. Ashcroft, N.W.; and Mermin, N.D.; Solid State Physics, Philadelphia, Pennsylvania: Saunders College, **1976**. **DOI**: 10.1002/piuz.19780090109
22. Mitchell, J. W.; and Goodrich, R. G.; *Phys. Rev. B*, **1985**, 32, 4969. **DOI**: 10.1103/PhysRevB.32.4969
23. Sancho-Parramon, J.; *Nanotechnology*, **2009,** 20, 235706. **DOI**: 10.1088/0957-4484/20/23/235706
24. King, S. R.; Massicot, J.; McDonagh, A. M.; *Metals*, **2015**, 5, 1454. **DOI**: 10.3390/met5031454
25. Mayer, M.; *Nucl. Instrum. Methods Phys. Res., Sect. B*, **2014**, 332, 176. **DOI**: 10.1016/j.nimb.2014.02.056

